

pubs.acs.org/Macromolecules Article

# Oligo(ethylene glycol) Side Chain Architecture Enables Alcohol-**Processable Conjugated Polymers for Organic Solar Cells**

Justin Neu, Stephanie Samson, Kan Ding, Jeromy James Rech, Harald Ade, and Wei You\*



Cite This: Macromolecules 2023, 56, 2092-2103



Article Recommendations

ACCESS I Metrics & More Supporting Information **HSP Solubility Sphere EtOH** C<sub>6</sub>H<sub>13</sub> PTQ-6bO CHCI3 PTQ10 Alcohol-Soluble \*Different

**Architectures** 

**PTQ10** 

ABSTRACT: Achieving green-solvent solubility of conjugated polymers in truly green solvents such as alcohols has proven to be a significant challenge. In this work, we report the synthesis and characterization of three conjugated polymers derived from poly[(thiophene)-alt-(6,7-difluoro-2-(2-hexyldecyloxy)quinoxaline)] (PTQ10) with the goal of developing derivates which are more green-solvent-processable. The traditional alkyl side chains are replaced by various oligo(ethylene glycol) (OEG) side chains of different architectures, including one linear and two branched, all of which contain six ethylene glycol repeating units. It is determined that the linear OEG side chain architecture, even when sufficiently long, will not give desired green-solvent solubility shown by a small solubility capacity  $(R_0)$ . However, branched OEG side chains significantly improve solubility as  $R_0$  was increased from 4.7 of PTQ10 to 11.9 of PTQ-6bO/6bO2. Although the solution states of the polymers were vastly different, the solid-state morphologies were more similar as all three OEG-based polymers retained a predominately face-on molecular orientation similar to PTQ10. It was demonstrated that PTQ-6O devices showed the most comparable power conversion efficiencies (PCEs) to PTQ10 in bulk heterojunction solar cells, while PTQ-6bO2 and PTQ-6bO showed poorer performances. With one extra carbon in the side chain, PTQ-6bO2 showed higher PCE than PTQ-6bO, attributed to the improved aggregation properties and solid-state morphology of PTQ-6bO2, highlighting the importance of OEG side chain architecture. This work serves to develop important guidelines for future alcohol-soluble materials for green-solvent-processed OPVs.

#### INTRODUCTION

Increasing demand for renewable energy sources as replacements for fossil fuels has accelerated the emergence of solar cell technology. Ideally, renewable energy sources should be cost-effective and result in a low environmental impact in its creation to be considered truly sustainable. 1,2 Bulk heterojunction (BHJ) organic photovoltaics (OPVs) have gained considerable attention over the past several decades as a promising technology for harvesting clean and renewable solar energy because of their attractive merits of lightweight, high flexibility, and suitability for large-scale solution-processed manufacturing.<sup>3,4</sup> Rapid progress has been made; for example, the record high power conversion efficiency (PCE) of small area single junction devices in research laboratories for OPVs have recently surpassed 19%.5 These impressive accomplishments are promising for the future commercial production. However, significant issues must still be overcome before OPVs can be considered truly sustainable. For example, one of the beneficial traits of polymer-based OPVs is solution processability, which can significantly lower production costs.<sup>6,7</sup> However, chlorinated solvents such as chloroform (CF) and chlorobenzene (CB) are the prevailing solvents used for processing the active layers; since these solvents are hazardous and harmful to human health and the environment, 8,9 they are clearly not viable toward realizing sustainable and commercially practical OPVs. 10,11 Thus, seeking environmentally benign solvents has become increasingly important as environmental impacts would be significantly increased if

Received: November 2, 2022 Revised: February 3, 2023 Published: March 2, 2023





Figure 1. Design and synthesis of the four polymers in this work: PTQ10, PTQ-66O, PTQ-6bO, and PTQ-6bO2.

polymer-based OPVs were manufactured on a commercial scale with environmentally harmful solvents.

There has been significant progress in transitioning away from halogenated solvents to nonhalogenated ones; for example, efficiency numbers have surpassed 17% using toluene as the processing solvent. <sup>12</sup> In addition, *o*-xylene and tetrahydrofuran (THF) have also been popular solvents of choice. 13-15 Furthermore, solvents such as 2-methyltetrahydrofuran (2-MeTHF), D-limonene, or p-cymene represent biorenewable alternatives to the previously mentioned solvents; 16 indeed, good efficiencies of over 10% can still be achieved when processing from these biorenewable solvents. 17-19 Although these solvent systems should mark a significant improvement when compared to chlorinated solvent processing, the ideal solvents would be simple alcohols such as ethanol (EtOH) and water, which can be considered to be the most environmentally favorable.<sup>20</sup> Although significant progress has been made, PCEs achieved from devices processed from alcohols are currently only 3%. 21 The drastic difference in performance between state-of-the-art devices processed from chlorinated solvents and devices from green solvents and alcohols is the primary gap that needs to be narrowed to fully realize sustainably processed OPVs.

The solubility of conjugated polymers in solvents is primarily determined by their side chains and aggregation characteristics; the latter is particularly important to achieve optimized morphology in BHJ to maximize the obtainable PCE. 18,19 Alkylated side chains are commonly employed to allow conjugated polymers to be processable in both halogenated and nonhalogenated aromatic solvents (such as CF or toluene). However, achieving solubility in truly green solvents such as alcohols has proven to be a significant challenge. There are two main techniques to impart solubility of conjugated polymers in green solvents: adding side chains which contain ionic groups or incorporating oligo(ethylene glycol) (OEG) side chains. 22-25 Earlier attempts using ionic groups produced poor efficiencies, likely due to the ionic groups often forming traps in the polymer-based BHJ solar cells. 26,27 Thus, nonionic ethylene-glycol-based side chains are preferably used to impart solubility in green solvents. Although

this method is well documented, there are very few alcohol-processable polymer donors, the most notable being PPDT2FBT-A. <sup>25,28,29</sup> Thus, general design knowledge regarding the incorporation of OEG side chains into conjugated polymers to achieve green-solvent processability has not yet been firmly established. In fact, few OEG side chain optimization efforts have been reported, primarily focusing on the length of the OEG side chain. <sup>21,30–32</sup> Ideally, design rules and structure—property relationships when OEG side chains are used in conjugated polymers need to be developed in a similar fashion to the prevailing alkylated side chains. <sup>33</sup> This should include investigating different configurations of OEG side chains and their impacts to develop coherent structure—morphology—performance relationships; such knowledge will establish guidelines for the future development of green-solvent-soluble conjugated materials.

Herein, we report the synthesis of three new conjugated polymers derived from poly[(thiophene)-alt-(6,7-difluoro-2-(2-hexyldecyloxy)quinoxaline)] (PTQ10) with the goal of developing PTQ derivates which are more green-solventprocessable. Specifically, traditional alkyl side chains in PTQ10 are replaced with various OEG side chains including one linear, and two branched, all of which contain six ethylene glycol repeat units. Hansen solubility parameters were then used to understand and quantify the solubilities imparted by the various side chains. The morphological properties in solution and solid states were studied and compared to PTQ10 to develop structure-property relationships upon the implementation of OEG side chains. Interestingly, the structure of the OEG side chain (even with the same number of ethylene glycol units) has a profound effect on solubility, solution and solid-state morphologies, and optical properties, all of which ultimately influence the photovoltaic performance of BHI solar cells with these polymers. This work serves to develop important guidelines for future alcohol-soluble materials for green-solvent-processed OPVs.

#### RESULTS AND DISCUSSION

**Design and Synthesis.** PTQ10 has attracted significant interest as it offers high PCEs while possessing a rather simple

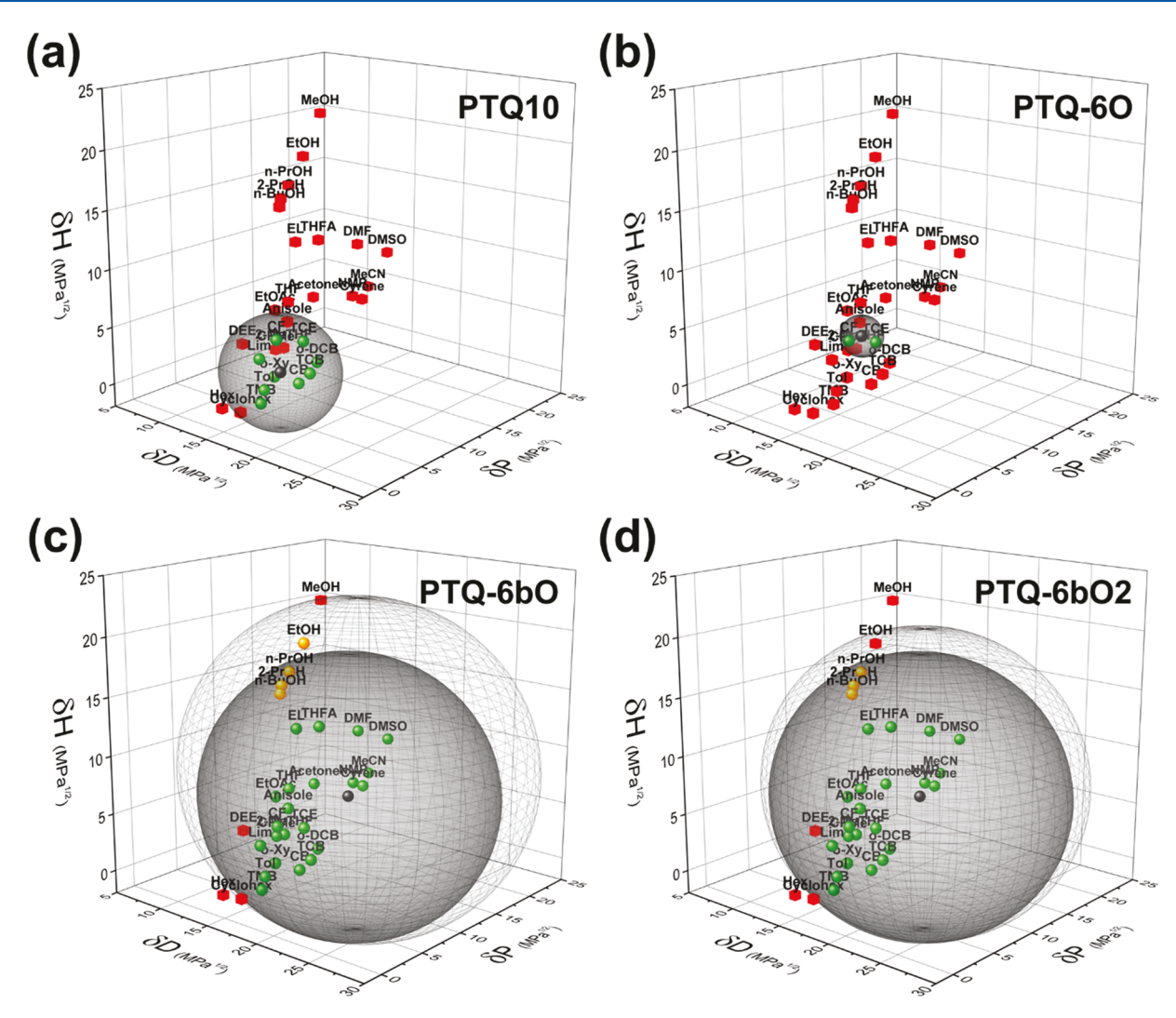


Figure 2. Solubility spheres determined at 10 mg/mL by HSP. Black represents the sphere center, green represents soluble at 25 °C (gray sphere), orange represents soluble at 60 °C (grid sphere), and red represents insoluble. (a) PTQ-10, (b) PTQ-60, (c) PTQ-6bO, and (d) PTQ-6bO2.

structure in comparison to other high-performance donor polymers.34-40 The obvious benefit toward synthesizing polymers with lower synthetic complexity is the significant reduction in material cost, energy expenditure, and produced wastes. These are important hurdles that should be considered when realizing commercially viable OPVs. In our previous work, the original synthesis of PTQ10 was redesigned, resulting in significant cost reduction (1/7th the original).<sup>41</sup> A key alteration in the synthesis was the use of Mitsunobu reaction to attach the solubilizing side chain, allowing for the use of alcohol-functionalized side chains instead of their brominated counterparts. This becomes particularly significant when looking to add OEG side chains as most are alcoholfunctionalized and bromination/tosylation would require further synthetic efforts. 42 Thus, this PTQ synthetic scaffold becomes an excellent way to attach various OEG side chains while maintaining the polymer backbone structure. Also, as the side chain of PTQ10 is attached via an oxygen-carbon bond to the conjugated backbone, potential electronic changes could be minimized as the OEG groups would maintain a similar attachment (Figure 1).

Thus, we chose PTQ10 as the platform to investigate the effects of solubility and morphology in solution and solid state upon implementation of various OEG side chains. Three new

derivatives were designed: one polymer bearing a linear OEG side chain with six ethylene glycol repeating units (thus PTQ-6O) and two bearing branched OEG side chains (PTQ-6bO and PTQ-6bO2) which differ in their branching point (1st or 2nd carbon, thus "O" and "O2" in the suffix). These structures were targeted to encompass a large breadth of different (yet related) side chain architectures that are commonly used. All polymers were designed to contain a total of six ethylene glycol repeat units to maintain approximately equal side chain content. The two different alcohol-functionalized branched OEG side chains were synthesized according to the previous literature. 32,43 All four monomers (including the original PTQ10 as the control) were synthesized via Mitsunobu reactions according to our previous report in yields ≥60% (synthetic details in the Supporting Information).<sup>41</sup> Finally, all polymers were synthesized via microwave-assisted Stille polymerization. The number-average molar mass  $(M_n)$  and dispersity (D) of the four polymers were measured by gel permeation chromatography (GPC). Synthetic details and corresponding characterizations are included in the Supporting Information. With the four polymers of interest synthesized, and motivated by the potential for green-solvent processability, we next investigated the solubility limits.

**Solubility Properties.** The solubility of conjugated polymers is commonly investigated through an empirical trial and error approach. Typically, the polymer of interest is put into different vials of various solvents and the solubility is directly investigated. Although this method does provide reasonable information about solubility, there is no predictive nature in this process. To improve upon this traditional practice of investigating solubility, a method which would predictively create a model of solubility became desired. Since Hansen Solubility Parameters (HSP) have been applied to various different types of systems, including the field of organic photovoltaics, <sup>19,44–50</sup> we applied HSP to quantitatively investigate and create a predictive model of solubility for the four PTQ polymers.

The HSP of PTQ10, PTQ-6O, PTQ-6bO, and PTQ-6bO2 were determined and plotted as a sphere of solubility along with various solvents of interest (Figure 2) (HSP determination described in the Supporting Information). The sphere is composed of a central coordinate with a radius defined as the solubility capacity ( $R_0$ ), representing the maximum distance between the center HSP coordinate and a solvent that enables the arbitrary solubility limit (e.g., 10 mg/mL). With the goal of processability in mind, the threshold of solubility was defined at 10 mg/mL. As a reference, the HSP ( $\delta_{\rm D}$ ,  $\delta_{\rm P}$ ,  $\delta_{\rm H}$ ) for PTQ10 were initially determined to be 19.2, 1.9, and 3.7, respectively, with an  $R_0$  of 4.7. The HSP for all other three polymers were similarly determined and all data are summarized in Table 1.

Table 1. Summary of the Determined Hansen Solubility Parameters of the Four PTQ Polymers at 25 °C

polymer	$\delta D  \left( \mathrm{MPa}^{1/2} \right)$	$\delta P  \left( \mathrm{MPa}^{1/2} \right)$	$\delta H \left( \mathrm{MPa}^{1/2} \right)$	$R_0$ (MPa <sup>1/2</sup> )
PTQ10	19.2	1.9	3.7	4.7
PTQ-6O	18.5	3.8	6.1	1.7
PTQ-6bO	19.5	9.7	7.0	11.9
PTQ-6bO2	19.5	9.7	7.0	11.9

PTQ10 expectedly yields solubility in chlorinated solvents and some nonchlorinated aromatic solvents commonly used for OPV processing (Figure 2a). Solubility in a desired solvent can be achieved in two ways; the first is by having very similar HSP coordinates, and the second by having a large  $R_0$  so that the solvent is encompassed within the solubility sphere. It is hypothesized that to gain solubility in solvents such as water or alcohols, the  $\delta_{\mathrm{P}}$  and  $\delta_{\mathrm{H}}$  of the polymers should be closer to those of the solvents. For example, the HSP coordinates of CF are 17.8, 3.1, and 5.7 while the coordinates of EtOH are 15.8, 8.8, and 19.4. Thus, it is expected that OEG side chains will increase the  $\delta_{\rm P}$  and  $\delta_{\rm H}$  values due to their higher polarity.<sup>50</sup> Indeed, the HSP were determined to be 18.5, 3.8, and 6.1, respectively, with an  $R_0$  of 1.7 for PTQ-6O with the linear OEG<sub>6</sub> side chain. This represents an increase in the  $\delta_P$  and  $\delta_H$ values by 1.9 and 2.4, respectively, in comparison to PTQ10. Although an increase in the  $\delta_{\rm p}$  and  $\delta_{\rm H}$  values is seen, a dramatic decrease in R<sub>0</sub> (Figure 2b) causes PTQ-6O to possess solubility in only CF and tetrachloroethane (TCE), which is worse in comparison to PTQ10. This dramatic decrease in the R<sub>0</sub> shows that the linear OEG<sub>6</sub> side chain is not a good architecture to provide improved solubility. On the other hand, the HSP were determined to be 19.5, 9.7, and 7.0, respectively, with an R<sub>0</sub> of 11.9 for the branched OEG polymers PTQ-6bO and PTQ-6bO2 at 25 °C. It is interesting to note that PTQ-6bO and PTQ-6bO2 were determined to have indistinguishable HSP at 25 °C, indicating that moving the branching point from the first carbon to the second does not have a major impact on the solubility of the polymer at 25 °C. Given the much improved  $\delta_P$  and  $\delta_H$  (as well as  $R_0$ ) for PTQ-6bO and PTQ-6bO2 with branched OEG6 side chains, these two polymers show a dramatic increase in the total solubility when compared to PTQ10 or PTQ-6O, indicating the importance of the side chain architecture and branching point on solubility. Interestingly, differences between PTQ-6bO and PTQ-6bO2 can be seen at higher temperatures (further HSP comparisons shown in the Supporting Information). According to the HSP prediction that was experimentally determined, PTQ-6bO would possess solubility in EtOH at 60 °C whereas PTQ-6bO2 would not. Indeed, our experimental results validated our prediction. We speculated that these differences in solubility are due to different aggregation characteristics between the represented polymers in solution, which we studied next.

Aggregation and Optical and Electrochemical Properties. Morphological optimization of the active layers in OPVs requires a comprehensive understanding of polymeraggregated structures in solution and solid states; optical spectroscopy is a common method used to investigate polymer aggregation in solution or film state.<sup>51</sup> The absorption of the four different polymers in CF solution is shown in Figure 3a. The parent polymer PTQ10 possesses a  $\lambda_{max}$  at 560 and 590 nm corresponding to the 0-1 and 0-0 vibronic transitions, with an absorbance onset at 635 nm. PTQ-6O shows a relatively similar absorbance profile to that of PTQ-10 with  $\lambda_{\rm max}$  at 563 and 593 nm, and an onset at 638 nm. This slight red-shift and increased 0-0/0-1 ratio of PTQ-6O is indicative of a slight increase in the conjugation length and increased aggregation of PTQ-6O in solution, which can be attributed to the reduction in sterics from the introduction of the linear OEG<sub>6</sub> side chain in comparison to the branched alkyl variant in PTQ10. Increased planarization and tighter packing of the polymer chains have been seen in another study where different branching points of alkyl chains of PTQ polymers were investigated. S2 However, the two polymers bearing branched OEG side chains produce vastly different absorption profiles in CF compared to PTQ10 or PTQ-6O. For example, PTQ-6bO possesses a single  $\lambda_{max}$  at 484 nm and an onset at 552 nm, representing an incredible 83 nm blue-shift in comparison to PTQ10. On the other hand, PTQ-6bO2 possesses a similar blue-shift, albeit to a lesser extent with a  $\lambda_{\rm max}$  at 514 and 564 nm, and an onset at 599 nm. As all of these polymers maintain the same backbone or "chromophore" component, differences in absorbance should be related to a change in the backbone planarity and aggregation behavior. Given that PTQ-6bO and PTQ-6bO2 show dramatic blue-shift when compared to PTQ10 and PTQ-6O, the former two polymers would possess significantly more disordered confirmations in CF solution.

As the two branched polymers have improved solubility as shown by the HSP spheres, the absorption of PTQ-6bO and PTQ-6bO2 was further investigated in various green-solvent alternatives. It can be seen that the optical properties of PTQ-6bO and PTQ-6bO2 are heavily solvent-dependent as the absorption changes significantly upon different solvent conditions (Figures 3b,c and S5). As various green-solvent systems are poorer solvents in comparison to CF, backbone planarization and aggregation are induced, <sup>53</sup> resulting in the red-shift for PTQ-6bO and PTQ-6bO2 (Figure 3b,c). By contrast, blue-shift in absorption is seen for the branched OEG

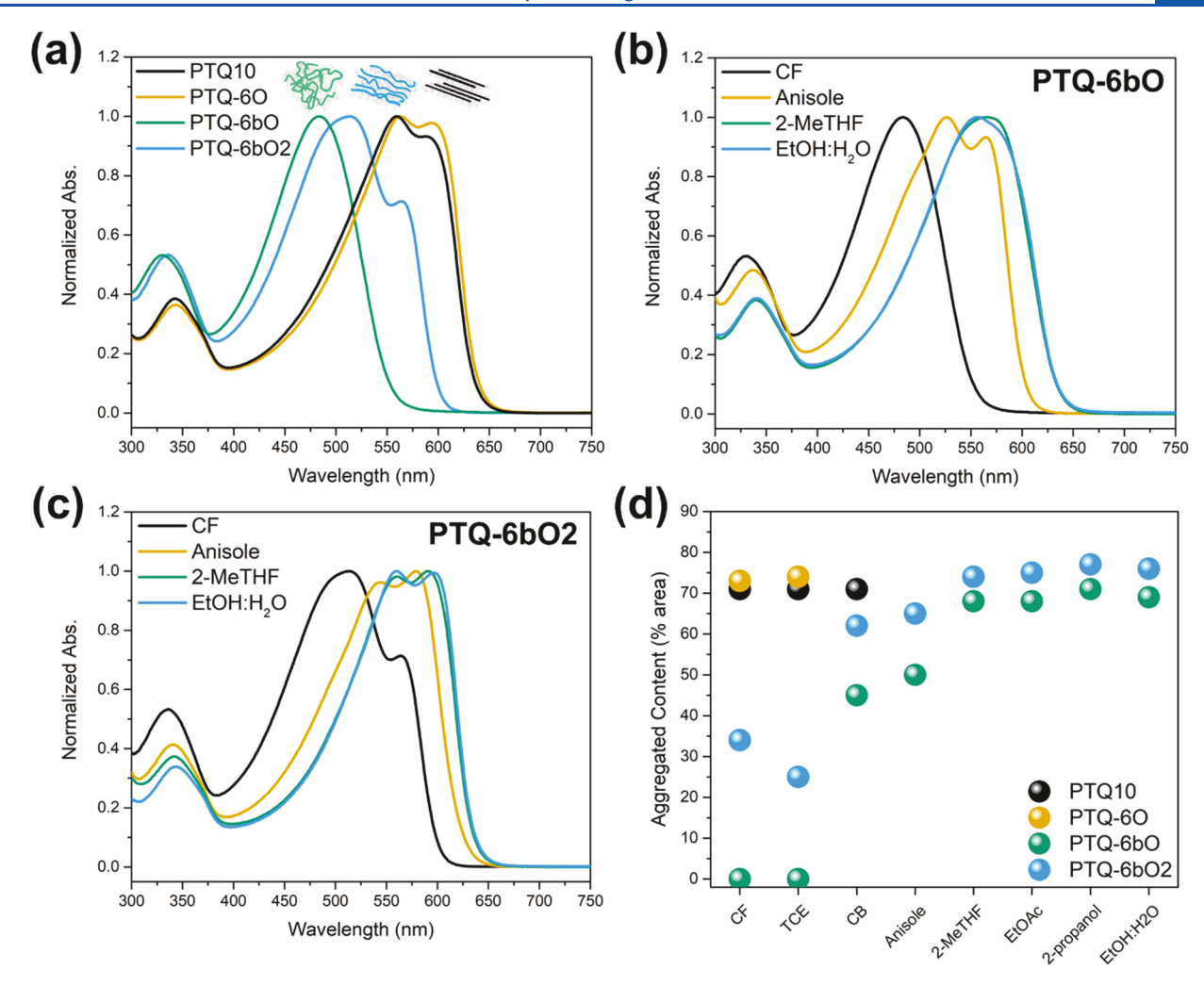


Figure 3. Normalized UV—vis absorption spectra in 25  $\mu$ g/mL solution. (a) All four polymers in CF; (b) PTQ-6bO and (c) PTQ-6bO2 in various solvents; (d) % area of aggregated content from deconvolution as described in the Supporting Information.

polymers in CF as the solubility for PTQ-6bO and PTQ-6bO2 is considerably higher in comparison to the linear OEG and alkyl counterparts (PTQ-6O and PTQ10). For example, PTQ-6bO exhibits a  $\lambda_{\text{max}}$  at 556 nm and an onset at 636 nm in a 25 v/v% H<sub>2</sub>O in EtOH solvent system (denoted as EtOH-H<sub>2</sub>O). Somewhat similarly, PTQ-6bO2 exhibits a  $\lambda_{max}$  at 560 and 597 nm with an onset at 636 nm in the EtOH-H<sub>2</sub>O solvent system. However, it can be seen that the absorption profiles of the two branched OEG polymers are slightly different as PTQ-6bO2 possesses more distinct vibronic transitions compared to PTQ-6bO. This could be attributed to a more increased order of the aggregates formed by PTQ-6bO2 as the branching point is moved away from the backbone, which would increase  $\pi$ – $\pi$ interactions. To gain a more quantitative understanding of the aggregation behavior of the polymers in different solvents, deconvolution was performed by subtracting the area of the disordered phase from the total spectrum to obtain the ordered component (deconvolution example given in Figure S6).<sup>54</sup> From this deconvolution, the % area of the aggregated component from the total spectrum was used as a simple method to quantitatively compare the aggregated content of the polymers in various solvents (Figure 3d). Unsurprisingly, PTQ-6O possesses slightly higher aggregated content in comparison to PTQ10. Also, PTQ-6bO and PTQ-6bO2 possess significantly lower amounts of the aggregated content

in CF compared to PTQ10, which is consistent with the aforementioned results. Interestingly, the amount of the aggregated content of PTQ-6bO and PTQ-6bO2 in more environmentally friendly solvents such as 2-MeTHF, EtOAc, and EtOH– $\rm H_2O$  are similar to PTQ10 in toxic, chlorinated solvents such as CF and CB. A complete summary of the optical properties in solution is given in Table S9. Notably, the aggregated content of PTQ-6bO2 is consistently higher than that of PTQ-6bO in all solvents investigated (Figure 3d), indicating that the branching point can impart subtle differences in the aggregation characteristics.

Further investigation was carried out to understand the differences in aggregation behavior as conjugated polymers are known to undergo an order—disorder transition in solution upon cooling. Thus, temperature-dependent UV—vis absorption measurements were conducted in 1,2-dichlorobenzene (o-DCB) and TCE (Figure S7a—h). At high temperatures, PTQ10 shows a featureless peak centered around 500 nm, corresponding to the disordered phase. Once cooled to around 125 °C, aggregate formation is seen and further cooling results in the continued planarization of the polymer backbone and further red-shifting (Figure S7a). A similar trend is seen with PTQ-6bO and PTQ-6bO2 in o-DCB (Figure S7c,d); however, the temperatures at which aggregate formations become discernable for these two polymers are significantly lower in

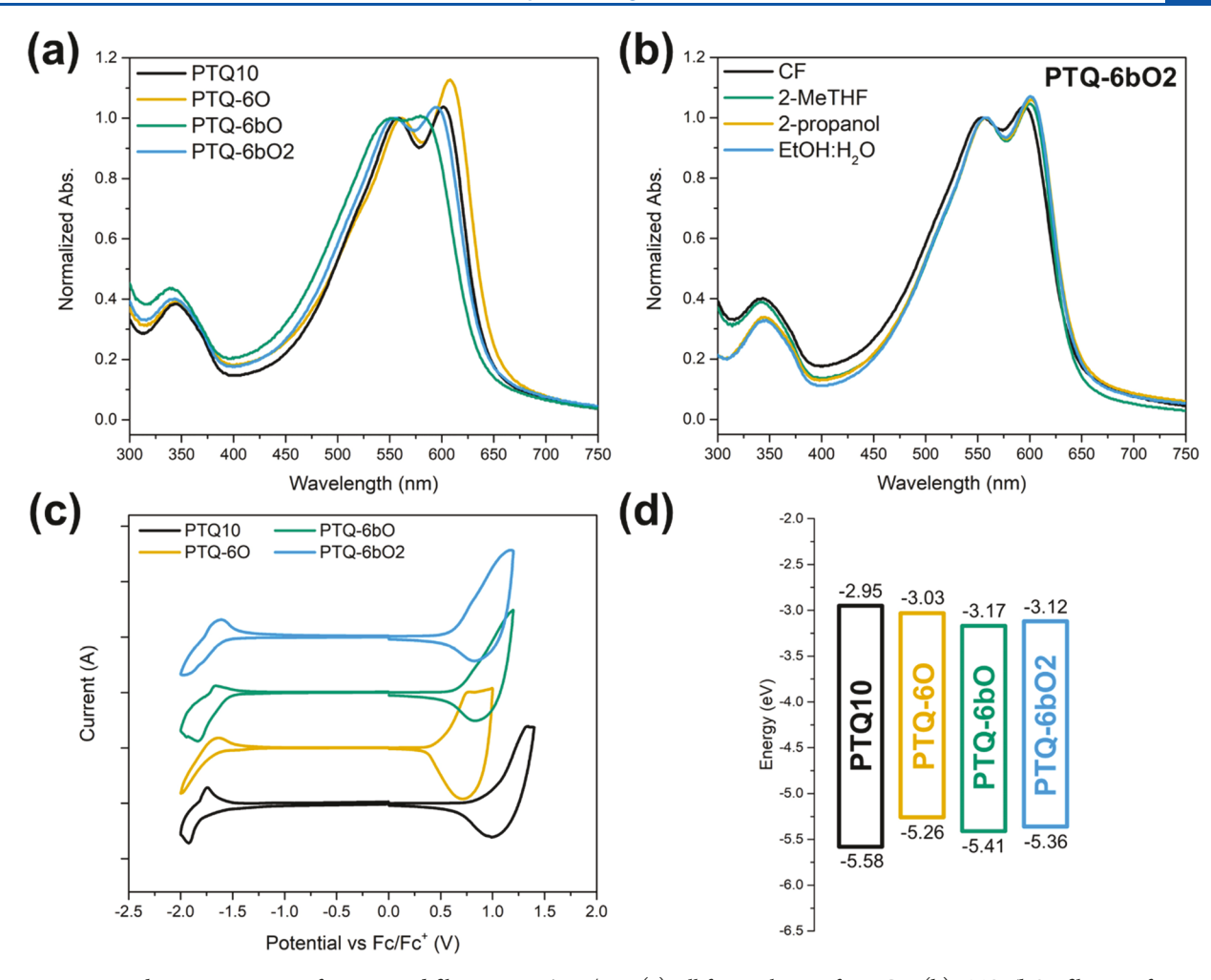


Figure 4. UV—vis absorption spectra of spin-coated films cast at 6 mg/mL. (a) All four polymers from CF; (b) PTQ-6bO2 film cast from various solvents; (c) cyclic voltammograms determined employing a 0.1 M tetrabutylammonium hexafluorophosphate in acetonitrile solution as the supporting electrolyte; and (d) energy levels determined by CV.

Table 2. Summary of the Optical and Electrochemical Properties of the Polymers Determined in CF Solution and Film States Cast from CF

	solı	ition				film		
polymer	$\lambda_{\max}^{Sol}$ (nm)	$\lambda_{\mathrm{onset}}^{\mathrm{Sol}}$ (nm)	$\lambda_{max}$ (nm)	$\lambda_{\text{onset}}$ (nm)	$E_{\rm g}^{\rm \; opt} \; ({\rm eV})$	HOMO <sup>a</sup> (eV)	LUMO <sup>b</sup> (eV)	$E_{\rm g}^{\ { m CV}}\ ({ m eV})$
PTQ10	560,590	635	558,601	642	1.93	-5.58	-2.95	2.63
PTQ-6O	563,593	638	561,608	648	1.91	-5.26	-3.03	2.23
PTQ-6bO	484	552	551,580	635	1.95	-5.41	-3.17	2.24
PTQ-6bO2	514,564	599	555,594	640	1.94	-5.36	-3.12	2.24

<sup>a</sup>Calculated from the  $E_{\rm OX}$ . <sup>b</sup>Calculated from the  $E_{\rm RED}$ . The  $E_{\rm OX}$  and  $E_{\rm RED}$  was determined employing a 0.1 M tetrabutylammonium hexafluorophosphate in acetonitrile solution as the supporting electrolyte.

comparison to PTQ10. A decrease in the aggregate formation temperature is attributed to an increase in the solubility of the branched OEG polymers by an increase in the side chain entropy. Although there are small differences between the three branched side chain polymers (alkyl or OEG), including differences in the temperature of aggregate deformation, the largest difference in temperature-dependent aggregation behavior is seen in PTQ-6O. As shown in Figure S7b, even at high temperatures, PTQ-6O never shows a blue-shift corresponding to the breakdown of the aggregation. The absorption onset and  $\lambda_{\rm max}$  remain mostly unchanged even at 150 °C. This further indicates the strong aggregation character of PTQ-6O due to the linear OEG side chain.

The absorption properties of all four polymers as thin films were further measured, which represent the aggregated polymers in the solid state. Differences in absorption profiles are still visible yet become more subtle as film drying kinetics tend to dominate over the confirmation of the polymer in solution (Figures 4a and S4c). Nevertheless, the same trends exist as in solution. PTQ10 shows a  $\lambda_{\rm max}$  at 558 and 601 nm with an onset of 642 nm in the film cast from CF; in comparison, PTQ-6O shows a slight red-shift with an onset of 648 nm with an increased 0–0/0–1 transition ratio relative to PTQ10. These observations are consistent with the results in solution. On the other hand, PTQ-6bO remains the most blueshifted among all four polymers with an onset at 635 nm.

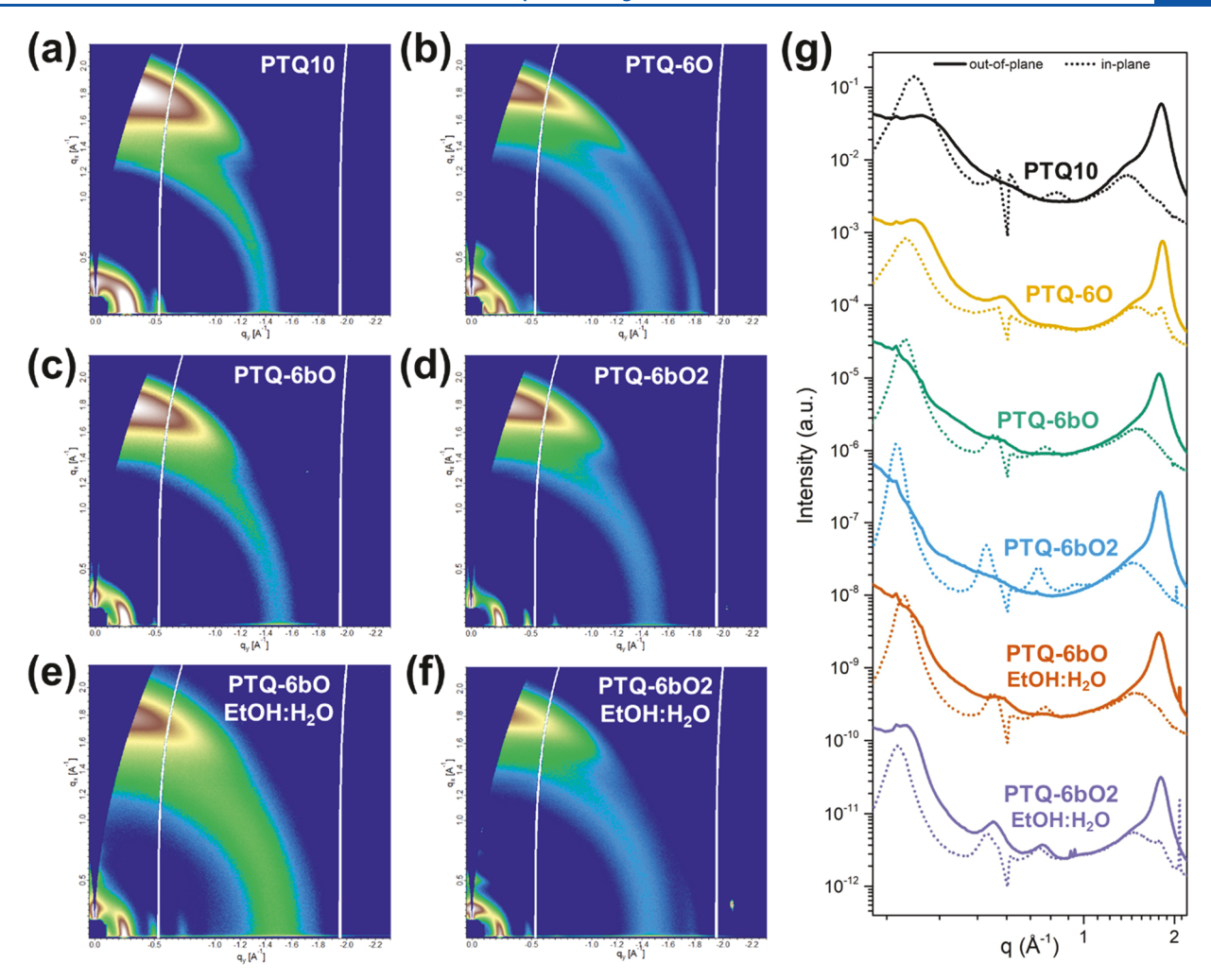


Figure 5. GIWAXS of neat polymer films cast from CF (a-d) or EtOH- $H_2O_{25\%}$  (e, f) and corresponding in-plane and out-of-plane line cut profiles (g). Note that the in-plane peak around 0.6 Å<sup>-1</sup> is an artifact of the measurement grid and cannot be removed.

Similar to the results in solution, the 0–0 and 0–1 transitions of PTQ-6bO are less distinct in comparison to the other polymers. This gives further evidence as PTQ-6bO possesses less ordered aggregation due to disruption induced by a branching point that is closer to the backbone. Further evidence to this claim can be seen from PTQ-6bO2; it exhibits an onset at 640 nm and more distinctive transitions which are more similar to PTQ10. All optical properties are summarized in Table 2.

As the two branched OEG polymers showed high solvent dependence in solution, the effects of different casting solvents were further investigated to study the solid-state morphology. Figure 4b shows the absorbance of PTQ-6bO2 in the film state processed from four different solvents: CF, 2-MeTHF, 2propanol, and EtOH-H2O. Although differences are more minor in comparison to solution, the films processed in the three green-solvent systems (2-MeTHF, 2-propanol, and EtOH-H<sub>2</sub>O) are marginally more red-shifted in comparison with that cast from CF. Regardless, the final absorption profile of PTQ-6bO2 is largely unchanged (i.e., independent of the processing solvent), which is also true for PTQ-6bO as similar results were obtained (Figure S8). This observation indicates that the casting solvent may not play a major role in controlling the morphology of the polymer under our experimental conditions, opening the choice of the processing solvent.

To evaluate the impact of different side chains on the energy levels of this PTQ series, we applied cyclic voltammetry (CV) to estimate the highest occupied molecular orbital (HOMO) and the lowest unoccupied molecular orbital (LUMO) energy levels (Figure 4c). The HOMO energy levels can be calculated from the conversion of the oxidation onset  $(E_{OX})$  through the ferrocene standard ( $E_{FC}$ ) using the equation HOMO = -(4.8)+  $(E_{\rm OX}-E_{\rm FC})$ ), and the LUMO can be found in a similar fashion using the reduction onset  $(E_{RED})$ . From the oxidation and reduction onsets, the HOMO and LUMO levels of PTQ10 were estimated to be -5.58 and -2.95 eV, respectively, and the energy levels of other three polymers were determined similarly. Interestingly, the HOMO and LUMO levels of all three OEG-bearing polymers narrow significantly in comparison to PTQ10, which has also been observed in other studies. 42,55,56 This is an unexpected result as the OEG side chains, from an electronic point of view, should be equal to an alkoxy group as both are linked to the aryl ring by an oxygen atom; thus, the energy levels of all four polymers would be expected to be very similar. Various interpretations have been proposed<sup>57,58</sup> to account for similar behaviors. For example, Roncali et al. argued that an increase in the ionic conductivity of the polymer via these OEG groups would assist the electrochemical doping process of conjugated polymers during the CV measurement and alter the obtained redox

potentials.<sup>57</sup> Furthermore, Johansson et al. proposed that the ion-complexing ability (among other factors) of OEGs could be more important than electronic effects in influencing the redox potentials of OEG-substituted polythiophenes.<sup>58</sup> Thus, caution should be taken when estimating the HOMO and LUMO energy levels of the three OEG polymers by CV. Nevertheless, the narrowed band gap of PTQ-6O as seen by UV—vis  $(E_{\rm g}^{\rm opt})$  is also corroborated by CV measurement  $(E_{\rm g}^{\rm CV})$  as this reduction is likely due to extensive aggregation of PTQ-6O.

Morphological Properties. To further evaluate the impact of the different OEG side chains on the molecular self-assembly orientational features of the films, grazing incidence wide-angle X-ray scattering (GIWAXS) was conducted for thin films of pure polymers (Figure 5) and their BHJ blends with ITIC as the acceptor (Figure S9). Interestingly, all films show a preferred face-on packing orientation in the vertical direction of the substrate, evidenced by the  $\pi$ – $\pi$  stacking (010) diffraction peak in the out-of-plane (OOP) direction and lamellar d-spacing peak (100) in the inplane direction (Figure 5a),<sup>37</sup> indicating that the various side chains do not have a major impact on the molecular orientations (Figure 5a-f). However, differences in the  $\pi$ - $\pi$ stacking and lamellar *d*-spacing are observed. The corresponding detailed data of peak analysis along in-plane (IP) and outof-plane (OOP) directions are depicted in Tables 3 and S11.

Table 3. GIWAXS Summary of Neat Polymer Films Annealed at 140  $^{\circ}$ C for 5  $\min^{a}$ 

	in-pla	ane (100)	out-of-plane (010)		
polymer film	$q_{xy}$ (Å <sup>-1</sup> )	d-spacing (Å)	$q_z \; (\mathring{\rm A}^{-1})$	$\pi$ – $\pi$ distance (Å)	
PTQ10 <sup>b</sup>	0.275	22.8	1.800	3.49	
PTQ-60 <sup>b</sup>	0.258	24.4	1.823	3.45	
РТQ-6bО <sup><i>b</i></sup>	0.256	24.5	1.775	3.54	
PTQ-6bO2 <sup>b</sup>	0.240	26.2	1.795	3.50	
PTQ-6bO <sup>c</sup>	0.253	24.8	1.774	3.54	
PTQ-6bO2 <sup>c</sup>	0.242	25.9	1.798	3.49	
- /			1.		

<sup>&</sup>lt;sup>a</sup>(100) along IP and (010) along OOP. <sup>b</sup>Films processed from CF. <sup>c</sup>Films processed from EtOH–H<sub>2</sub>O<sub>25%</sub>.

For example, when processed in CF, PTQ10 shows a  $\pi-\pi$ stacking distance of 3.49 Å, whereas PTQ-6O has a corresponding distance of 3.45 Å. A smaller  $\pi - \pi$  stacking distance for PTQ-6O is expected, as there should be a reduction in the sterics of the linear OEG side chain compared to one that is branched. On the other hand, an increased  $\pi - \pi$ stacking distance of 3.54 Å is observed for PTQ-6bO than the observed 3.50 Å for PTQ-6bO2, as the side chain branch point is closer to the polymer backbone in the case of PTQ-6bO and offers more steric hindrance. These trends in the  $\pi$ - $\pi$  stacking distances are in agreement with the results obtained from UVvis, where the absorption peaks of the films with smaller  $\pi$ – $\pi$ stacking distances are red-shifted compared with those with larger  $\pi$ – $\pi$  stacking distances. Expected trends are also seen for the lamellar *d*-spacing distances. For example, with the shortest length of branch (C10), PTQ10 possesses the smallest lamellar d-spacing distances of 22.8 Å, whereas PTQ-6bO with the "C13" side chain as the longest branch (from the O attached to the quinoxaline core) shows longer lamellar d-spacing distances of 24.5 Å. Interestingly, PTQ-6O with even longer "C19" has a similar distance of 24.4 Å to that of PTQ-6bO, which could be attributed to increased interdigitation of the

linear OEG side chains in comparison to the branched variants. Finally, with one more carbon longer than in its side chain than that of PTQ-6bO, PTQ-6bO2 shows the largest lamellar dspacing distance of 26.2 Å when processed from CF.<sup>59</sup> Furthermore, to investigate the effects of different processing solvents, films of PTQ-6bO and PTQ-6bO2 cast from an EtOH-H<sub>2</sub>O cosolvent mixture were also subject to GIWAXS characterization. Contrary to previous reports, 25 no significant changes in the neat polymer film morphology were seen upon casting from different solvents. For example, when processed from EtOH– $H_2O$ , PTQ-6bO possesses the same  $\pi$ – $\pi$  stacking distance of 3.54 Å compared to CF, and only a marginally increased lamellar d-spacing distance of 24.8 Å was observed. On the other hand, PTQ-6bO2 (processed from EtOH-H<sub>2</sub>O) possesses a  $\pi - \pi$  stacking distance of 3.49 Å and a lamellar dspacing distance of 25.9 Å. This insensitivity to processing solvent condition of PTQ-6bO and PTQ-6bO2 is interesting, especially considering the vastly different polymer conformations seen in solution previously shown by UV-vis. However, this insensitivity may be beneficial for future green-solvent processing as in an ideal case, the morphology would remain consistent even upon different processing solvents.

**Photovoltaic Properties.** To investigate how the aforementioned properties of these polymers impact device efficiency, all four polymers were employed as the donor in BHJ solar cells with ITIC as the acceptor, with a device architecture of ITO/PEDOT:PSS/PTQ donor:ITIC/PDINO/Al (active area of 6.8 mm²). ITIC was chosen as the acceptor material to match with the PTQ polymers as it has been previously investigated with PTQ10,<sup>60</sup> and serves as a consistent control to investigate the different photovoltaic properties. The *J-V* curves are shown in Figure 6. The

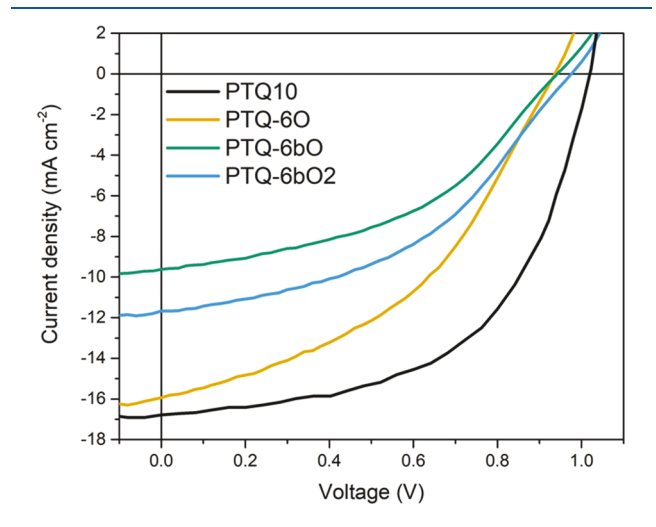


**Figure 6.** *J*–*V* curves of optimized PTQ–ITIC devices cast from CF.

PTQ10:ITIC reference device achieved a PCE of 9.5% at the optimized annealing condition of 140 °C for 5 min. From the UV—vis data of pure polymers (Figure 4a), it would be expected that PTQ-6O could show the most comparable PCE to PTQ10 as its aggregation character is the most similar to PTQ10 in CF, potentially resulting in the most similar morphology for their BHJ blends. As shown by the GIWAXS data, the morphology of the BHJ blend of PTQ10:ITIC is most comparable to that of PTQ-6O:ITIC, while the PTQ-6bO:ITIC and PTQ-6bO2:ITIC blends show more significant changes (Figure S9 and Table S12). Indeed, the PTQ-

Table 4. Summary of the Photovoltaic Properties for the PTQ-Based PSCs

polymer	processing solvent	$J_{\rm SC} \pm \sigma  ({\rm mA/cm^2})^a$	$V_{\rm OC} \pm \sigma  (V)^a$	$FF \pm \sigma (\%)^a$	PCE $\pm \sigma$ (best) (%) <sup>a</sup>
PTQ10 <sup>b</sup>	CF	$16.46 \pm 0.15$	$1.02 \pm 0.00$	$55.6\% \pm 1.0$	$9.3\% \pm 0.1\% (9.5)$
PTQ-60 <sup>c</sup>	CF	$15.81 \pm 0.38$	$0.93 \pm 0.00$	$41.7\% \pm 1.1$	$6.2\% \pm 0.3\% (6.4)$
PTQ-6bO <sup>€</sup>	CF	$9.30 \pm 0.29$	$0.92 \pm 0.01$	$44.3\% \pm 1.3$	$3.8\% \pm 0.2\% (4.1)$
	2-MeTHF	$8.20 \pm 0.19$	$0.97 \pm 0.01$	$32.4\% \pm 0.8$	$2.6\% \pm 0.1\% (2.7)$
	anisole	$6.71 \pm 0.40$	$0.96 \pm 0.01$	$33.3\% \pm 0.7$	$2.1\% \pm 0.2\% (2.3)$
PTQ-6bO2 <sup>d</sup>	CF	$10.86 \pm 0.77$	$0.96 \pm 0.03$	$43.5\% \pm 0.8$	$4.5\% \pm 0.5\% (5.0)$

<sup>a</sup>Optimized devices with an architecture of ITO/PEDOT:PSS/PTQ donor:ITIC/PDINO/Al (estimated from at least four devices with an active area of 6.8 mm²). <sup>b</sup>D:A weight ratio of 1:1, annealed at 140 °C for 5 min. <sup>c</sup>D:A weight ratio of 1:1, annealed at 125 °C for 5 min.

6O:ITIC device performed the best of the OEG-based materials, achieving a PCE of 6.4%. On the other hand, since the film absorption profiles of PTQ-6bO2 and PTQ-6bO show more amorphous conformations compared to PTQ10 (Figure 4a), it was assumed that BHJ devices comprising these two polymers would likely show lower PCEs. Indeed, this trend was found to be true as PTQ-6bO:ITIC and PTQ-6bO2:ITIC devices achieved PCEs of 4.1 and 5.0%, respectively (Tables 4 and S13). Importantly, our results show that the subtle optimization of the OEG side chains can result in improved device performance as PTQ-6bO2 consistently shows improved PCE over PTQ-6bO.

Owing to the increased solubility of the PTQ polymers bearing branched OEG side chains (PTQ-6bO and PTQ-6bO2) in green solvents, we wanted to investigate the impact on device performance when casting the active layer from greener solvent systems, including 2-MeTHF and anisole. As PTQ-6bO showed the best solubility, this material was chosen. For simple comparison, the same device architecture as previously stated was maintained, with the only difference being the casting solvent. It should be noted that upon the dissolution of PTQ-6bO and ITIC in 2-MeTHF/anisole, significant aggregation was observed. This can be largely attributed to the acceptor due to the poorer solubility of ITIC in 2-MeTHF/anisole when compared to CF. However, heating the solution to 60 °C can alleviate this issue. PCEs of 2.7 and 2.3% were achieved for PTQ-6bO:ITIC devices from 2-MeTHF and anisole, respectively (Table 4 and Figure S10). Compared to the CF devices, the 2-MeTHF and anisole devices both showed decreases in the short circuit current  $(J_{SC})$  and fill factor (FF).

The consistent decrease in the PCE of devices with the OEG-based donor polymers (with ITIC as the acceptor) when compared to the reference polymer PTQ10 is intriguing. We hypothesize that this decrease in performance is related to the blend morphology and miscibility between the OEG-based polymers and ITIC. As demonstrated from our HSP analysis above, the OEG-based PTQ polymers have much higher  $\delta_{\rm P}$ and  $\delta_{\rm H}$  parameters when compared to PTQ10. It can be expected that common acceptors bearing alkyl side chains such as ITIC or Y6 have closer  $\delta_{\rm P}$  and  $\delta_{\rm H}$  parameters to more traditional, alkyl-based donors, which would lead to improved miscibility of these donor/acceptor pairs.<sup>61</sup> Poor miscibility between the donor and acceptor will likely result in significant phase separation, becoming detrimental to device performance (particularly to  $J_{SC}$  and FF, as seen in Table 4). If the trend of the HSP parameters of the polymers is considered, the device results correlate well as PTQ-6O, compared with PTQ-6bO or PTQ-6bO2, is more similar to PTQ10. However, more indepth investigation is needed to fully understand how the

miscibility of the two materials changes with the incorporation of OEG side chains. Importantly, the poor device performance of PTQ-6bO (an OEG-modified donor) and ITIC (an alkylated acceptor) emphasizes the need for developing acceptors with improved miscibility with the OEG-based polymers to further explore the potential of green-solvent-processed OPVs. Although there have been efforts in making EtOH–H<sub>2</sub>O soluble acceptors with OEG side chains, previous work has focused on the PCBM or N2200 platform. As the state-of-the-art high-efficiency BHJ solar cells almost exclusively employ Y-series acceptors, synthetic efforts should be directed to developing high-performance EtOH–H<sub>2</sub>O soluble Y-series acceptors with OEG side chains.

#### CONCLUSIONS

In summary, three new conjugated polymers (i.e., PTQ-6O, PTQ-6bO, and PTQ-6bO2) derived from PTQ10 were synthesized by replacing traditional alkyl side chains with polar, OEG side chains of various architectures. Hansen solubility parameters were used to understand and differentiate solubility differences between the various side chains while creating predictive solubility models for green-solvent selection. It was determined that the linear OEG side chain architecture, even when sufficiently long, will not give desired green-solvent solubility shown by a small R<sub>0</sub>. However, branched OEG side chains are able to significantly improve solubility as the  $R_0$  was increased from 4.7 of PTQ10 to 11.9 of PTQ-6bO/6bO2. The poor solubility of PTQ-6O with a linear OEG side chain is attributed to strong aggregation character in solution. Meanwhile, the branched OEG polymers PTQ-6bO and PTQ-6bO2 were significantly more disordered in CF solution and displayed heavily solvent-dependent aggregation characteristics. Although the solution states of the polymers were vastly different, the solid-state morphologies were rather similar. All three OEG-based polymers retained a predominately face-on molecular orientation similar to PTQ10, and PTQ-6bO and PTQ-6bO2 even retained a relatively similar morphology when processed in a green solvent (EtOH $-H_2O$ ). With ITIC as the acceptor, PTQ-6O devices showed the most comparable performance to PTQ10, while PTQ-6bO2 and PTQ-6bO showed poorer performances. However, PTQ-6bO2 showed improved performance over PTQ-6bO, which can be attributed to improved aggregation properties and the solidstate morphology of PTQ-6bO2. Taken all together, it becomes clear that the architecture of the OEG side chain has a profound effect on solubility, solution/solid-state morphologies, and photovoltaic performance. This work can serve as important guidelines for the future design of alcoholsoluble materials for green-solvent-processed OPVs. Future work should focus on the synthesis of an alcohol-processable

small-molecule acceptor to match with these polymers, ultimately striving for high-performance alcohol-processed OPVs

#### ASSOCIATED CONTENT

### Supporting Information

The Supporting Information is available free of charge at https://pubs.acs.org/doi/10.1021/acs.macromol.2c02259.

Methods; detailed experimental procedures; and additional data (PDF)

#### AUTHOR INFORMATION

#### **Corresponding Author**

Wei You — Department of Chemistry and Department of Applied Physical Sciences, University of North Carolina at Chapel Hill, Chapel Hill, North Carolina 27599, United States; orcid.org/0000-0003-0354-1948; Email: wyou@unc.edu

#### **Authors**

Stephanie Samson – Department of Applied Physical Sciences, University of North Carolina at Chapel Hill, Chapel Hill, North Carolina 27599, United States

Kan Ding – Department of Physics and ORaCEL, North Carolina State University, Raleigh, North Carolina 27695, United States

Jeromy James Rech — Department of Chemistry, University of North Carolina at Chapel Hill, Chapel Hill, North Carolina 27599, United States; Occid.org/0000-0001-7963-9357

Harald Ade – Department of Physics and ORaCEL, North Carolina State University, Raleigh, North Carolina 27695, United States

Complete contact information is available at: https://pubs.acs.org/10.1021/acs.macromol.2c02259

#### Notes

The authors declare no competing financial interest.

## **■** ACKNOWLEDGMENTS

This work was financially supported by the National Science Foundation (NSF) under Award CBET-1934374 (to W.Y.) and CBET-1934351 (to H.A.). NMR Spectrometers were supported by the National Science Foundation under Grant No. CHE-0922858 and CHE-1828183. We thank Eliza Neidhart of Frank Leibfarth's lab at UNC and Ethan Stinchcomb of Jason Locklin's lab at UGA for use of their GPCs.

#### REFERENCES

- (1) Espinosa, N.; Hösel, M.; Angmo, D.; Krebs, F. C. Solar Cells with One-Day Energy Payback for the Factories of the Future. *Energy Environ. Sci.* **2012**, *5*, 5117–5132.
- (2) Riede, M.; Spoltore, D.; Leo, K. Organic Solar Cells—The Path to Commercial Success. *Adv. Energy Mater.* **2021**, *11*, No. 2002653.
- (3) Inganäs, O. Organic Photovoltaics over Three Decades. *Adv. Mater.* **2018**, *30*, No. 1800388.
- (4) Heeger, A. J. 25th Anniversary Article: Bulk Heterojunction Solar Cells: Understanding the Mechanism of Operation. *Adv. Mater.* **2014**, *26*, 10–28.

- (5) Zhu, L.; Zhang, M.; Xu, J.; Li, C.; Yan, J.; Zhou, G.; Zhong, W.; Hao, T.; Song, J.; Xue, X.; Zhou, Z.; Zeng, R.; Zhu, H.; Chen, C. C.; MacKenzie, R. C. I.; Zou, Y.; Nelson, J.; Zhang, Y.; Sun, Y.; Liu, F. Single-Junction Organic Solar Cells with over 19% Efficiency Enabled by a Refined Double-Fibril Network Morphology. *Nat. Mater.* **2022**, *21*, *656–663*.
- (6) Hong, L.; Yao, H.; Cui, Y.; Ge, Z.; Hou, J. Recent Advances in High-Efficiency Organic Solar Cells Fabricated by Eco-Compatible Solvents at Relatively Large-Area Scale. *APL Mater.* **2020**, *8*, 120901.
- (7) Wang, G.; Adil, M. A.; Zhang, J.; Wei, Z. Large-Area Organic Solar Cells: Material Requirements, Modular Designs, and Printing Methods. *Adv. Mater.* **2019**, *31*, No. 1805089.
- (8) Larsen, C.; Lundberg, P.; Tang, S.; Ràfols-Ribé, J.; Sandström, A.; Mattias Lindh, E.; Wang, J.; Edman, L. A Tool for Identifying Green Solvents for Printed Electronics. *Nat. Commun.* **2021**, *12*, 4510.
- (9) Byrne, F. P.; Jin, S.; Paggiola, G.; Petchey, T. H. M.; Clark, J. H.; Farmer, T. J.; Hunt, A. J.; Robert McElroy, C.; Sherwood, J. Tools and Techniques for Solvent Selection: Green Solvent Selection Guides. *Sustain. Chem. Process.* **2016**, *4*, 1–24.
- (10) Fan, B.; Zhang, D.; Li, M.; Zhong, W.; Zeng, Z.; Ying, L.; Huang, F.; Cao, Y. Achieving over 16% Efficiency for Single-Junction Organic Solar Cells. *Sci. China Chem.* **2019**, *62*, 746–752.
- (11) Yuan, J.; Zhang, Y.; Zhou, L.; Zhang, G.; Yip, H. L.; Lau, T. K.; Lu, X.; Zhu, C.; Peng, H.; Johnson, P. A.; Leclerc, M.; Cao, Y.; Ulanski, J.; Li, Y.; Zou, Y. Single-Junction Organic Solar Cell with over 15% Efficiency Using Fused-Ring Acceptor with Electron-Deficient Core. *Joule* 2019, 3, 1140–1151.
- (12) Xu, X.; Yu, L.; Yan, H.; Li, R.; Peng, Q. Highly Efficient Non-Fullerene Organic Solar Cells Enabled by a Delayed Processing Method Using a Non-Halogenated Solvent. *Energy Environ. Sci.* **2020**, *13*, 4381–4388.
- (13) Hong, L.; Yao, H.; Wu, Z.; Cui, Y.; Zhang, T.; Xu, Y.; Yu, R.; Liao, Q.; Gao, B.; Xian, K.; Woo, H. Y.; Ge, Z.; Hou, J. Eco-Compatible Solvent-Processed Organic Photovoltaic Cells with Over 16% Efficiency. *Adv. Mater.* **2019**, *31*, No. 1903441.
- (14) Dong, S.; Jia, T.; Zhang, K.; Jing, J.; Huang, F. Single-Component Non-Halogen Solvent-Processed High-Performance Organic Solar Cell Module with Efficiency over 14%. *Joule* **2020**, *4*, 2004–2016.
- (15) Cui, Y.; Yao, H.; Hong, L.; Zhang, T.; Xu, Y.; Xian, K.; Gao, B.; Qin, J.; Zhang, J.; Wei, Z.; Hou, J. Achieving Over 15% Efficiency in Organic Photovoltaic Cells via Copolymer Design. *Adv. Mater.* **2019**, 31, No. 1808356.
- (16) Clarke, C. J.; Tu, W. C.; Levers, O.; Bröhl, A.; Hallett, J. P. Green and Sustainable Solvents in Chemical Processes. *Chem. Rev.* **2018**, *118*, 747–800.
- (17) Li, Z.; Ying, L.; Zhu, P.; Zhong, W.; Li, N.; Liu, F.; Huang, F.; Cao, Y. A Generic Green Solvent Concept Boosting the Power Conversion Efficiency of All-Polymer Solar Cells to 11%. *Energy Environ. Sci.* **2019**, *12*, 157–163.
- (18) Zhu, L.; Zhong, W.; Qiu, C.; Lyu, B.; Zhou, Z.; Zhang, M.; Song, J.; Xu, J.; Wang, J.; Ali, J.; Feng, W.; Shi, Z.; Gu, X.; Ying, L.; Zhang, Y.; Liu, F. Aggregation-Induced Multilength Scaled Morphology Enabling 11.76% Efficiency in All-Polymer Solar Cells Using Printing Fabrication. *Adv. Mater.* 2019, 31, No. 1902899.
- (19) Ye, L.; Xiong, Y.; Chen, Z.; Zhang, Q.; Fei, Z.; Henry, R.; Heeney, M.; O'Connor, B. T.; You, W.; Ade, H. Sequential Deposition of Organic Films with Eco-Compatible Solvents Improves Performance and Enables Over 12%-Efficiency Nonfullerene Solar Cells. Adv. Mater. 2019, 31, No. 1808153.
- (20) Capello, C.; Fischer, U.; Hungerbühler, K. What Is a Green Solvent? A Comprehensive Framework for the Environmental Assessment of Solvents. *Green Chem.* **2007**, *9*, 927–993.
- (21) Shang, L.; Qu, S.; Deng, Y.; Gao, Y.; Yue, G.; He, S.; Wang, Z.; Wang, Z.; Tan, F. Simple Furan-Based Polymers with the Self-Healing Function Enable Efficient Eco-Friendly Organic Solar Cells with High Stability. *J. Mater. Chem. C* **2022**, *10*, 506–516.
- (22) Mwaura, J. K.; Pinto, M. R.; Witker, D.; Ananthakrishnan, N.; Schanze, K. S.; Reynolds, J. R. Photovoltaic Cells Based on

- Sequentially Adsorbed Multilayers of Conjugated Poly(p-Phenylene Ethynylene)s and a Water-Soluble Fullerene Derivative. *Langmuir* **2005**, *21*, 10119–10126.
- (23) Yang, J.; Garcia, A.; Nguyen, T. Q. Organic Solar Cells from Water-Soluble Poly(Thiophene)/Fullerene Heterojunction. *Appl. Phys. Lett.* **2007**, *90*, 2005–2008.
- (24) Duan, C.; Cai, W.; Hsu, B. B. Y.; Zhong, C.; Zhang, K.; Liu, C.; Hu, Z.; Huang, F.; Bazan, G. C.; Heeger, A. J.; Cao, Y. Toward Green Solvent Processable Photovoltaic Materials for Polymer Solar Cells: The Role of Highly Polar Pendant Groups in Charge Carrier Transport and Photovoltaic Behavior. *Energy Environ. Sci.* **2013**, *6*, 3022–3034.
- (25) Nguyen, T. L.; Lee, C.; Kim, H.; Kim, Y.; Lee, W.; Oh, J. H.; Kim, B. J.; Woo, H. Y. Ethanol-Processable, Highly Crystalline Conjugated Polymers for Eco-Friendly Fabrication of Organic Transistors and Solar Cells. *Macromolecules* **2017**, *50*, 4415–4424.
- (26) Duan, C.; Zhang, K.; Zhong, C.; Huang, F.; Cao, Y. Recent Advances in Water/Alcohol-Soluble  $\pi$ -Conjugated Materials: New Materials and Growing Applications in Solar Cells. *Chem. Soc. Rev.* **2013**, *42*, 9071–9104.
- (27) Lee, S.; Jeong, D.; Kim, C.; Lee, C.; Kang, H.; Woo, H. Y.; Kim, B. J. Eco-Friendly Polymer Solar Cells: Advances in Green-Solvent Processing and Material Design. *ACS Nano* **2020**, *14*, 14493–14527.
- (28) Kim, C.; Kang, H.; Choi, N.; Lee, S.; Kim, Y.; Kim, J.; Wu, Z.; Woo, H. Y.; Kim, B. J. C70-Based Aqueous-Soluble Fullerene for the Water Composition-Tolerant Performance of Eco-Friendly Polymer Solar Cells. J. Mater. Chem. C 2020, 8, 15224–15233.
- (29) Lee, C.; Lee, H. R.; Choi, J.; Kim, Y.; Nguyen, T. L.; Lee, W.; Gautam, B.; Liu, X.; Zhang, K.; Huang, F.; Oh, J. H.; Woo, H. Y.; Kim, B. J. Efficient and Air-Stable Aqueous-Processed Organic Solar Cells and Transistors: Impact of Water Addition on Processability and Thin-Film Morphologies of Electroactive Materials. *Adv. Energy Mater.* **2018**, *8*, No. 1802674.
- (30) Jeong, D.; Jo, I. Y.; Lee, S.; Kim, J. H.; Kim, Y.; Kim, D.; Reynolds, J. R.; Yoon, M. H.; Kim, B. J. High-Performance n-Type Organic Electrochemical Transistors Enabled by Aqueous Solution Processing of Amphiphilicity-Driven Polymer Assembly. *Adv. Funct. Mater.* **2022**, 32, No. 2111950.
- (31) Chen, Z.; Yan, L.; Rech, J. J.; Hu, J.; Zhang, Q.; You, W. Green-Solvent-Processed Conjugated Polymers for Organic Solar Cells: The Impact of Oligoethylene Glycol Side Chains. *ACS Appl. Polym. Mater.* **2019**, *1*, 804–814.
- (32) Lee, S.; Kim, Y.; Wu, Z.; Lee, C.; Oh, S. J.; Luan, N. T.; Lee, J.; Jeong, D.; Zhang, K.; Huang, F.; Kim, T. S.; Woo, H. Y.; Kim, B. J. Aqueous-Soluble Naphthalene Diimide-Based Polymer Acceptors for Efficient and Air-Stable All-Polymer Solar Cells. ACS Appl. Mater. Interfaces 2019, 11, 45038–45047.
- (33) Liu, Y.; Zhao, J.; Li, Z.; Mu, C.; Ma, W.; Hu, H.; Jiang, K.; Lin, H.; Ade, H.; Yan, H. Aggregation and Morphology Control Enables Multiple Cases of High-Efficiency Polymer Solar Cells. *Nat. Commun.* **2014**, *5*, 5293.
- (34) Huang, H.; Huang, H.; Li, X.; Li, X.; Sun, C.; Sun, C.; Angunawela, I.; Qiu, B.; Qiu, B.; Du, J.; Du, J.; Qin, S.; Qin, S.; Meng, L.; Zhang, Z.; Ade, H.; Li, Y.; Li, Y.; Li, Y. Green Solvent-Processed Organic Solar Cells Based on a Low Cost Polymer Donor and a Small Molecule Acceptor. *J. Mater. Chem. C* 2020, 8, 7718–7724.
- (35) Sun, C.; Pan, F.; Bin, H.; Zhang, J.; Xue, L.; Qiu, B.; Wei, Z.; Zhang, Z. G.; Li, Y. A Low Cost and High Performance Polymer Donor Material for Polymer Solar Cells. *Nat. Commun.* **2018**, *9*, 743.
- (36) Chai, G.; Chang, Y.; Zhang, J.; Xu, X.; Yu, L.; Zou, X.; Li, X.; Chen, Y.; Luo, S.; Liu, B.; Bai, F.; Luo, Z.; Yu, H.; Liang, J.; Liu, T.; Wong, K. S.; Zhou, H.; Peng, Q.; Yan, H. Fine-Tuning of Side-Chain Orientations on Nonfullerene Acceptors Enables Organic Solar Cells with 17.7% Efficiency. *Energy Environ. Sci.* 2021, 14, 3469–3479.
- (37) Sun, C.; Pan, F.; Chen, S.; Wang, R.; Sun, R.; Shang, Z.; Qiu, B.; Min, J.; Lv, M.; Meng, L.; Zhang, C.; Xiao, M.; Yang, C.; Li, Y. Achieving Fast Charge Separation and Low Nonradiative Recombination Loss by Rational Fluorination for High-Efficiency Polymer Solar Cells. *Adv. Mater.* **2019**, *31*, No. 1905480.

- (38) Cha, H.; Zheng, Y.; Dong, Y.; Lee, H. H.; Wu, J.; Bristow, H.; Zhang, J.; Lee, H. K. H.; Tsoi, W. C.; Bakulin, A. A.; McCulloch, I.; Durrant, J. R. Exciton and Charge Carrier Dynamics in Highly Crystalline PTQ10:IDIC Organic Solar Cells. *Adv. Energy Mater.* 2020, 10, No. 2001149.
- (39) Li, S.; Zhan, L.; Sun, C.; Zhu, H.; Zhou, G.; Yang, W.; Shi, M.; Li, C. Z.; Hou, J.; Li, Y.; Chen, H. Highly Efficient Fullerene-Free Organic Solar Cells Operate at Near Zero Highest Occupied Molecular Orbital Offsets. *J. Am. Chem. Soc.* **2019**, *141*, 3073–3082.
- (40) Cheng, H. W.; Juan, C. Y.; Mohapatra, A.; Chen, C. H.; Lin, Y. C.; Chang, B.; Cheng, P.; Wang, H. C.; Chu, C. W.; Yang, Y.; Wei, K. H. High-Performance Organic Photovoltaics Incorporating an Active Layer with a Few Nanometer-Thick Third-Component Layer on a Binary Blend Layer. *Nano Lett.* **2021**, *21*, 2207–2215.
- (41) Rech, J. J.; Neu, J.; Qin, Y.; Samson, S.; Shanahan, J.; Josey, R. F.; Ade, H.; You, W. Designing Simple Conjugated Polymers for Scalable and Efficient Organic Solar Cells. *ChemSusChem* **2021**, *14*, 3561–3568.
- (42) Chen, X.; Zhang, Z.; Ding, Z.; Liu, J.; Wang, L. Diketopyrrolopyrrole-Based Conjugated Polymers Bearing Branched Oligo(Ethylene Glycol) Side Chains for Photovoltaic Devices. *Angew. Chem., Int. Ed.* **2016**, *55*, 10376–10380.
- (43) Leal-Duaso, A.; Pérez, P.; Mayoral, J. A.; Garciá, J. I.; Pires, E. Glycerol-Derived Solvents: Synthesis and Properties of Symmetric Glyceryl Diethers. ACS Sustainable Chem. Eng. 2019, 7, 13004–13014
- (44) Graham, K. R.; Wieruszewski, P. M.; Stalder, R.; Hartel, M. J.; Mei, J.; So, F.; Reynolds, J. R. Improved Performance of Molecular Bulk-Heterojunction Photovoltaic Cells through Predictable Selection of Solvent Additives. *Adv. Funct. Mater.* **2012**, *22*, 4801–4813.
- (45) Burgués-Ceballos, I.; Machui, F.; Min, J.; Ameri, T.; Voigt, M. M.; Luponosov, Y. N.; Ponomarenko, S. A.; Lacharmoise, P. D.; Campoy-Quiles, M.; Brabec, C. J. Solubility Based Identification of Green Solvents for Small Molecule Organic Solar Cells. *Adv. Funct. Mater.* **2014**, 24, 1449–1457.
- (46) Zhao, K.; Zhang, Q.; Chen, L.; Zhang, T.; Han, Y. Nucleation and Growth of P(NDI2OD-T2) Nanowires via Side Chain Ordering and Backbone Planarization. *Macromolecules* **2021**, *54*, 2143–2154.
- (47) Bin, H.; Yang, Y.; Zhang, Z. G.; Ye, L.; Ghasemi, M.; Chen, S.; Zhang, Y.; Zhang, C.; Sun, C.; Xue, L.; Yang, C.; Ade, H.; Li, Y. 9.73% Efficiency Nonfullerene All Organic Small Molecule Solar Cells with Absorption-Complementary Donor and Acceptor. *J. Am. Chem. Soc.* 2017, 139, 5085–5094.
- (48) Leman, D.; Kelly, M. A.; Ness, S.; Engmann, S.; Herzing, A.; Snyder, C.; Ro, H. W.; Kline, R. J.; DeLongchamp, D. M.; Richter, L. J. In Situ Characterization of Polymer-Fullerene Bilayer Stability. *Macromolecules* **2015**, *48*, 383–392.
- (49) Kim, N. K.; Shin, E. S.; Noh, Y. Y.; Kim, D. Y. A Selection Rule of Solvent for Highly Aligned Diketopyrrolopyrrole-Based Conjugated Polymer Film for High Performance Organic Field-Effect Transistors. *Org. Electron.* **2018**, *55*, 6–14.
- (50) Lee, J.; Park, S. A.; Ryu, S. U.; Chung, D.; Park, T.; Son, S. Y. Green-Solvent-Processable Organic Semiconductors and Future Directions for Advanced Organic Electronics. *J. Mater. Chem. A* **2020**, *8*, 21455–21473.
- (51) Panzer, F.; Bässler, H.; Köhler, A. Temperature Induced Order-Disorder Transition in Solutions of Conjugated Polymers Probed by Optical Spectroscopy. *J. Phys. Chem. Lett.* **2017**, *8*, 114–125.
- (52) Yuan, D.; Qin, G.; Zhang, L.; Pan, F.; Qiu, R.; Lei, S.; Deng, S.; Chen, J. Delicately Controlled Polymer Orientation for High-Performance Non-Fullerene Solar Cells with Halogen-Free Solvent Processing. ACS Appl. Mater. Interfaces 2021, 13, 57654–57663.
- (53) Scharsich, C.; Lohwasser, R. H.; Sommer, M.; Asawapirom, U.; Scherf, U.; Thelakkat, M.; Neher, D.; Köhler, A. Control of Aggregate Formation in Poly(3-Hexylthiophene) by Solvent, Molecular Weight, and Synthetic Method. J. Polym. Sci., Part B: Polym. Phys. 2012, 50, 442–453.
- (54) Steyrleuthner, R.; Schubert, M.; Howard, I.; Klaumünzer, B.; Schilling, K.; Chen, Z.; Saalfrank, P.; Laquai, F.; Facchetti, A.; Neher,

Macromolecules Article pubs.acs.org/Macromolecules

- D. Aggregation in a High-Mobility n-Type Low-Bandgap Copolymer with Implications on Semicrystalline Morphology. J. Am. Chem. Soc. **2012**, 134, 18303-18317.
- (55) Brebels, J.; Douvogianni, E.; Devisscher, D.; Thiruvallur Eachambadi, R.; Manca, J.; Lutsen, L.; Vanderzande, D.; Hummelen, J. C.; Maes, W. An Effective Strategy to Enhance the Dielectric Constant of Organic Semiconductors-CPDTTPD-Based Low Bandgap Polymers Bearing Oligo (Ethylene Glycol) Side Chains. J. Mater. Chem. C 2018, 6, 500-511.
- (56) Meng, B.; Song, H.; Chen, X.; Xie, Z.; Liu, J.; Wang, L. Replacing Alkyl with Oligo(Ethylene Glycol) as Side Chains of Conjugated Polymers for Close  $\pi$ - $\pi$  Stacking. Macromolecules 2015, 48, 4357-4363.
- (57) Roncali, J.; Garreau, R.; Delabouglise, D.; Garnier, F.; Lemaire, M. Modification of the Structure and Electrochemical Properties of Poly(Thiophene) by Ether Groups. J. Chem. Soc., Chem. Commun. 1989, 11, 679-681.
- (58) Johansson, T.; Mammo, W.; Svensson, M.; Andersson, M. R.; Inganäs, O. Electrochemical Bandgaps of Substituted Polythiophenes. J. Mater. Chem. 2003, 13, 1316-1323.
- (59) Liu, C.; Xiao, C.; Wang, J.; Liu, B.; Hao, Y.; Guo, J.; Song, J.; Tang, Z.; Sun, Y.; Li, W. Revisiting Conjugated Polymers with Long-Branched Alkyl Chains: High Molecular Weight, Excellent Mechanical Properties, and Low Voltage Losses. Macromolecules 2022, 55, 5964-5974.
- (60) Xu, Z.; Pan, F.; Sun, C.; Hong, S.; Chen, S.; Yang, C.; Zhang, Z.; Liu, Y.; Russell, T. P.; Li, Y.; Wang, D. Understanding the Morphology of High-Performance Solar Cells Based on a Low-Cost Polymer Donor. ACS Appl. Mater. Interfaces 2020, 12, 9537-9544.
- (61) Corzo, D.; Rosas-Villalva, D.; Amruth, C.; Tostado-Blázquez, G.; Alexandre, E. B.; Hernandez, L. H.; Han, J.; Xu, H.; Babics, M.; De Wolf, S.; Baran, D. High-Performing Organic Electronics Using Terpene Green Solvents from Renewable Feedstocks. Nat. Energy **2023**, 8, 62–73.
- (62) Li, S.; Li, C. Z.; Shi, M.; Chen, H. New Phase for Organic Solar Cell Research: Emergence of Y-Series Electron Acceptors and Their Perspectives. ACS Energy Lett. 2020, 5, 1554-1567.

# **□** Recommended by ACS

Facile Synthesis of Key Building Blocks of D18 Series Conjugated Polymers for High-Performance Polymer Solar Cells

Xiaowei Zhong, Wei You, et al.

FEBRUARY 09, 2023

ACS APPLIED POLYMER MATERIALS

RFAD 🗹

**Electron-Transporting Conjugated Polymers from Novel Aromatic Five-Membered Diimides: Naphtho**[1,2-b:4,3-b']dithiophene and -Diselenophene Diimides

Lingli Zhao, Huajie Chen, et al.

APRIL 05, 2023

MACROMOLECULES

READ

Double-Cable Conjugated Polymers Based on Simple Non-**Fused Electron Acceptors for Single-Component Organic Solar Cells** 

Baiqiao Liu, Weiwei Li, et al.

JANUARY 26, 2023

MACROMOLECULES

READ **C** 

New Type of Polymerized Small A-D-A Acceptors Constructed by Conjugation Extension in the Branched **Direction** 

Kangqiao Ma, Yongsheng Chen, et al.

FEBRUARY 22, 2023

ACS MATERIALS LETTERS

READ **C** 

Get More Suggestions >